PHOTONIC BANDGAPS

Inverse design of a pyrochlore lattice of DNA origami through model-driven experiments

Hao Liu[1], Michael Matthies[1], John Russo[2], Lorenzo Rovigatti[2], Raghu Pradeep Narayanan[1,3], Thong Diep[1], Daniel McKeen[4], Oleg Gang[4,5,6], Nicholas Stephanopoulos[1], Francesco Sciortino[2], Hao Yan[1], Flavio Romano[7,8], Petr Šulc[1,9]*

Sophisticated statistical mechanics approaches and human intuition have demonstrated the possibility of self-assembling complex lattices or finite-size constructs. However, attempts so far have mostly only been successful in silico and often fail in experiment because of unpredicted traps associated with kinetic slowing down (gelation, glass transition) and competing ordered structures. Theoretical predictions also face the difficulty of encoding the desired interparticle interaction potential with the experimentally available nano- and micrometer-sized particles. To overcome these issues, we combine SAT assembly (a patchy-particle interaction design algorithm based on constrained optimization) with coarse-grained simulations of DNA nanotechnology to experimentally realize trap-free self-assembly pathways. We use this approach to assemble a pyrochlore three-dimensional lattice, coveted for its promise in the construction of optical metamaterials, and characterize it with small-angle x-ray scattering and scanning electron microscopy visualization.

Nano- and microscopic structures can be realized through self-assembly, in which the building blocks are specifically designed to spontaneously aggregate into the target structure. Self-assembly has often been most successfully realized for the formation of two-dimensional (2D) structures, where the assembly process is directed by interactions of particles or molecules with the surfaces rather than the interparticle interactions. Extending self-assembly to three dimensions for nanostructures can be more challenging as several potential pitfalls can considerably lower the yield of the desired structure: (i) Metastable states can compete with the final product; (ii) dynamically arrested states (kinetic traps) can hinder assembly; (iii) low aggregation rates can slow the process; and (iv) lack of knowledge of the underlying phase behavior of the building blocks, especially for mixtures with many components, can lead to undesired products. From an experimental point of view, appropriate building blocks must be synthesized, and their size and interaction polydispersity, as well as their mechanical and molecular properties, such as softness and flexibility, can affect self-assembly in ways that are difficult to take into account in theoretical modeling.

Progress has also been hindered by the lack of a general framework for discovering designs that can self-assemble with high yield without encountering kinetic traps or unwanted [illegible] products. Some of the proposed solutions to this problem include statistical mechanical approaches (*1*–*11*), machine learning–inspired protocols (*12*), and optimization methods (*13*). So far, these approaches have been mostly in silico, with experiments relying more heavily on ingenious intuition (*14*–*18*), or painstakingly difficult trial-and-error attempts.

Here we use the synergy between theory, simulations, and experiments to address the aforementioned problems for the case of colloidal assembly. We introduce a new modeling-driven design pipeline based on patchy particles as building blocks. Patchy particles are micro- or nanoscale colloids that have anisotropic surface chemistry to direct bonding or have an anisotropic shape to direct assembly. Experimentally synthesized colloidal particles, capable of forming addressable directional bonds for self-assembly (*17*, *19*–*22*), can be modeled as patchy particles (*23*) for computational study. In our research, "patchy particles" specifically serve as a representation of wireframe DNA origami nanostructures (*24*), where a scaffold is constructed with single-stranded overhangs (sticky sequences), located in controllable positions, which can control the interaction between different patches. We show that our approach, which couples optimization methods

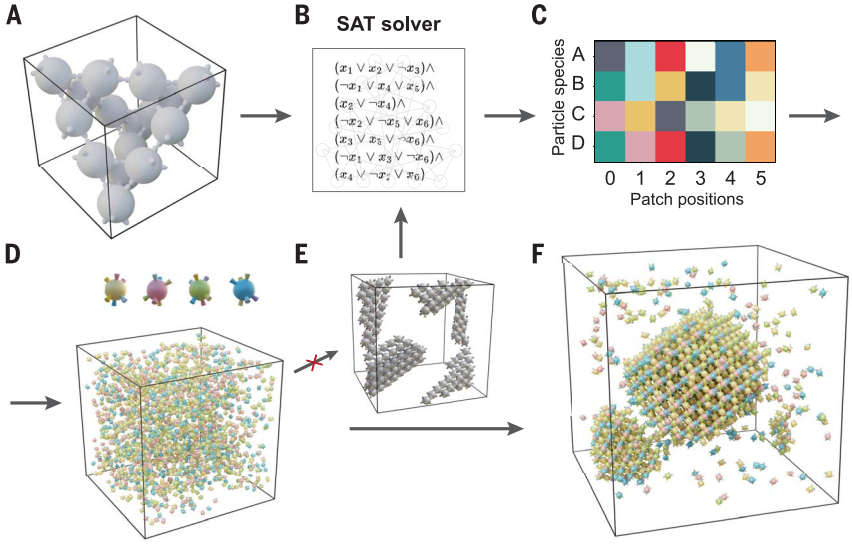

Fig. 1. Workflow of the computational design with SAT assembly. A) The topology of the unit cell of a pyrochlore lattice, where each particle has six neighbors. (**B**) The design problem to find a fixed number of species of patchy particles that satisfy the unit cell lattice is translated into a set of Boolean clauses [shown schematically here and listed in SM section S1]. (**C**) From the defined clauses, the SAT solver generates an interaction matrix corresponding to the assignment of colors to patches on respective species of patchy particles that can be arranged to satisfy the unit lattice interactions. (**D**) We simulate the bulk assembly of patchy particles in a range of temperatures and screen for undesired assemblies that prevent the formation of the desired lattice. (**E**) The identified undesired states are included as negative design in the SAT solver pipeline, explicitly banning solutions that can form these competing states. (**F**) The process is iterated until we find a patchy assignment that only results in successful nucleation and assembly of the desired lattice.

[1]School of Molecular Sciences and Center for Molecular Design and Biomimetics, The Biodesign Institute, Arizona State University, 1001 South McAllister Avenue, Tempe, AZ 85281, USA. [2]Dipartimento di Fisica, Sapienza Università di Roma, P.le Aldo Moro 5, 00185 Rome, Italy. [3]Department of Cellular and Molecular Pharmacology, University of California–San Francisco, San Francisco, CA 94143, USA. [4]Department of Chemical Engineering, Columbia University, 817 SW Mudd, New York, NY 10027, USA. [5]Department of Applied Physics and Applied Mathematics, Columbia University, New York, NY 10027, USA. [6]Center for Functional Nanomaterials, Brookhaven National Laboratory, Upton, NY 11973, USA. [7]Department of Molecular Sciences and Nanosystems, Ca' Foscari University of Venice, Via Torino 155, 30171 Venezia-Mestre, Italy. [8]European Centre for Living Technology (ECLT), Ca' Bottacin, 3911 Dorsoduro Calle Crosera, 30123 Venice, Italy. [9]School of Natural Sciences, Department of Bioscience, Technical University Munich, 85748 Garching, Germany.
*Corresponding author. Email: psulc@asu.edu

with multiscale simulations, actively shapes the design of DNA origami to realize the target structure with self-assembly.

As a test case, we focus on the pyrochlore (tetrastack) lattice, which so far has not been successfully experimentally realized by self-assembly. The pyrochlore lattice should have an omnidirectional photonic bandgap that is both wide and robust with respect to lattice defects (*25*, *26*). However, top-down fabrication methods, such as lithography, face practical limitations for manufacturing 3D structures at scales relevant for manipulating visible-light wavelengths, as they allow only for successive iterations of 2D patterning. Self-assembly offers a promising alternative, providing precise dimensional control at submicrometer scales with the aid of meticulously engineered building blocks. Nevertheless, realizing the pyrochlore lattice by self-assembly is particularly challenging owing to the existence of various competing structures that share similar bonding patterns but differ in stacking orders (*27*), impeding experimental realization to date. Notable attempts include the realization of binary Laves structures (*28*), encompassing both pyrochlore and cubic diamond sublattices, using tetrahedral clusters functionalized by DNA brushes (*26*, *29*), but the individual sublattices could not be isolated. Here, we successfully realized the colloidal pyrochlore lattice with DNA origami nanostructures. To further demonstrate the versatility of our method, we used two different DNA origami wireframe nanostructure designs (icosahedral and octahedral shapes, respectively) and show that they both robustly self-assemble into the pyrochlore superlattice, as confirmed by small-angle x-ray scattering (SAXS) and scanning electron microscopy (SEM) of the silica-coated lattice.

Inverse design in silico

We developed a multiscale approach to design DNA nanoparticles (NPs) and test in silico their assembly into the pyrochlore lattice (Fig. 1). We used the SAT-assembly method, which maps the inverse design problem to a Boolean satisfiability problem, also known as "SAT." First, we employed the method for interaction designs that include positive constraints (to ensure the interactions can satisfy the bonds in the desired lattice) as well as negative constraints (to exclude formation of competing structures). The second step was to numerically investigate the assembly process based on a coarse-grained patchy-particle model. Each NP is represented as a sphere with colored interaction sites, and only compatible colors can form a bond. The colors represent single-stranded DNA sequences, where compatible colors correspond to complementary sequences. If the simulations revealed the presence of unwanted competing structures, these were translated into additional negative constraints that were fed back to the optimization solver to look for solutions that exclude these competing states. This feedback loop was iterated until we obtained a solution for which the simulations produce the target structure with a high yield. The last step used nucleotide-level modeling that translated the patchy-particle design into a DNA origami amenable to experimental realization.

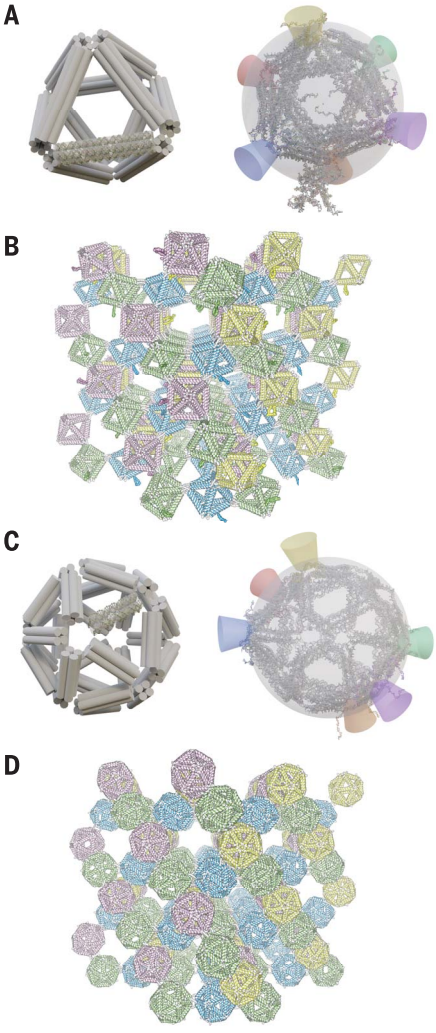

Fig. 2. Transferring the patchy particle design to the sequence design of DNA nanostructures with oxDNA simulations of the assembled lattice. (**A**) Octahedral and (**C**) icosahedral DNA origami are selected for the experimental implementation of patchy particles, with patches realized as single-stranded overhangs. Both structures have multihelical bundle edges to ensure their structural rigidity. We ran large-scale oxDNA simulations of large clusters (consisting of 128 DNA origami) with pyrochlore lattice geometry to ensure that the lattices are mechanically stable for chosen single-stranded overhang placements and lengths. The mean structures produced from the oxDNA simulations are shown in (**B**) and (**D**), respectively.

SAT assembly

The goal of the SAT-assembly procedure was to assign an interaction matrix that sets whether there is an attraction between any pair of building blocks such that the target lattice assembles without any kinetic traps or alternative free-energy minima that would lead to misassembled structures or defects in the lattice. The number of possible ways to design interaction matrices between patchy particles explodes combinatorially with an increasing number of possible colors and particle species, which in turn makes the search of the design space very challenging. To find an interaction matrix that can avoid these trapped states, we used the SAT-assembly framework (*13*, *30*) to formulate the design task as a SAT problem for which highly optimized solvers are available (*31*), allowing us to efficiently find solutions to the design problem.

These solutions were represented as a set of binary variables that specified which color was assigned to which patch, and which colors could interact. It further specified restrictions that the interactions needed to satisfy in terms of binary logic clauses composed of AND and OR and negation operations on the binary variables. These restrictions included that each color could only have one complementary color, each patch could only be assigned one color, and that the patchy particles could be arranged into the unit lattice so that all the patches on each particle were bound to a patch of complementary color [see supplementary material (SM) section S1 for details]. Thus, as a positive design task, we specified in terms of binary variables and logic clauses that the target lattice is an energy minimum of the patchy particle system, and let the SAT solver find color interactions and a patch color assignment that satisfy this condition. The first step of the SAT-assembly method was to specify the target unit cell of the lattice (Fig. 1). In the case of the pyrochlore lattice, the unit cell was composed of 16 individual particles, where each particle has six neighbors.

Patchy-particle simulations

We next verified that the solutions found by the SAT solver could homogeneously nucleate a pyrochlore crystal through molecular dynamics simulations (Fig. 1). The goal of our pipeline was to realize the building blocks with DNA origami nanostructures. For simulations of DNA nanotechnology, we typically used a nucleotide-level coarse-grained model, oxDNA (*32*–*35*), which can reproduce the structural, mechanical, and thermodynamic properties of single- and double-stranded DNA. However, the oxDNA model was too slow to simulate the kinetics of assembly of individual origami into

the lattice, so we used a coarser model in which the individual DNA nanostructures were represented as patchy spheres (Fig. 1D).

Each patch was assigned a color, as given by the solution from SAT solver. If two colors were compatible, they were considered to correspond to complementary single-stranded DNA overhangs and, in the patchy representation, to a short-range attractive potential. The spheres interacted with excluded volume interactions to prevent two particles from overlapping with each other. We have used the oxDNA model to parameterize the patchy particle model (SM section S1).

We ran multiple patchy-particle simulations in a range of temperatures to probe the assembly kinetics for each possible solution (see SM section S1 for details). Because of the highly coarse-grained nature of the patchy particle model, it is not possible to establish a direct one-to-one correspondence between the simulation temperature and the temperature in the experiment. However, we perform a range of simulations starting at high temperature (where no multiparticle structure forms, corresponding to an experimental temperature where no patch-patch bond between DNA origami is formed), all the way to low temperature, where every bond is effectively irreversible (corresponding to a case where every formed bond between complementary strands does not dissociate, and the system aggregates). For a working solution, we expect to observe in the simulation a nucleation event somewhere between these two limiting temperature cases. We first tried two solutions that used only one type of particle (with one and three colors, respectively), but our simulations show that it always leads to misassembled states. At high temperatures, the assembly remained in the gas phase, whereas at low temperatures, the system formed a quenched glassy state. At intermediate temperatures, where nucleation and assembly of the lattice should occur, the system formed misassembled states (Fig. 1E and fig. S2) stabilized by two bonds between two complementary pairs of patches on two patchy particles.

As a first iteration of the feedback loop, we introduced a negative design requirement that no pair of particles could bind to each other by more than one bond. In this way, we explicitly prevented the formation of the misassembled state above. For our pyrochlore lattice design, the SAT solver proved that no solution existed that satisfied the conditions above if we allowed only one patchy-particle species. Thus, we explored multicomponent systems with at least two particle types (SM section S1).

In multicomponent systems, we could add an additional requirement that a particle cannot form any bond with a particle of the same species. In the context of DNA origami interacting through single-stranded overhangs, this requirement will be shown to prevent possible aggregations or blocking by unpaired staple strands when each DNA nanostructure is prepared individually. SAT showed that this requirement suppressed all solutions with only two particle species, and that the smallest number of distinct particle species required is four (SM section S1).

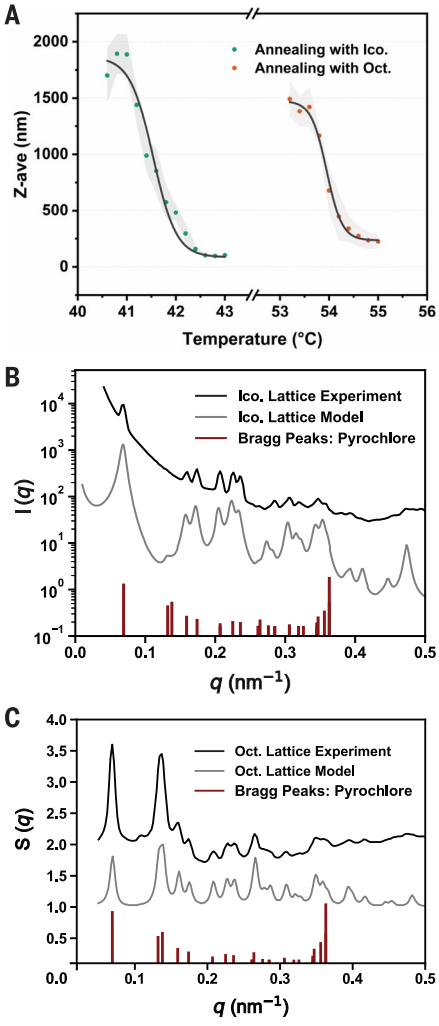

Fig. 3. Probing the self-assembly of the DNA origami building blocks for the pyrochlore lattice. (**A**) Dynamic light scattering as a function of temperature during the lattice assemblies (from icosahedral and octahedral DNA origami, respectively), used to identify the approximate assembly temperature. Experimental characterizations of the pyrochlore lattices with SAXS with (**B**) icosahedral and (**C**) octahedral building blocks. In black lines, we show the scattered intensity for lattice of icosahedral DNA origami in (B), and structure factors are shown in (C) for the lattice of octahedral origami with encaged gold nanoparticles. The SAXS measurements are compared to the predicted scattering model for DNA origami arranged in the pyrochlore lattice (gray lines) and the Bragg peak positions (red lines).

Our simulations showed that kinetic traps formed when a small number of colors was used. To decrease the chance of kinetic traps, we then set the solver to find solutions with the maximum number of colors, 24 (that is, 12 pairs of complementary colors). The resulting interaction matrix between patches is shown in Fig. 1C. Simulations confirmed the successful assembly of the 24-color solution into the desired pyrochlore lattice (Fig. 1F).

Realization of patchy particles with DNA nanotechnology

We next designed nucleic acid nanostructures that realized the patchy particles and their interactions found by the SAT assembly and verified with simulations of patchy particles (Fig. 2). We used the oxDNA model and interactive modeling tool oxView (*36*) to design DNA nanostructures to represent the patchy particles with wireframe DNA origami, where patches correspond to single-stranded overhangs with spacers (Fig. 2 and fig. S3). We considered two DNA wireframe origami designs: an icosahedral shape based on origami used in (*37*) (Fig. 2C), and a second one based on an octahedral origami from (*38*) (Fig. 2A). In the icosahedral origami, each patch corresponded to three single-stranded overhangs ("handles") placed in the vertex of the DNA origami, which made the overall geometry fully compatible with the corresponding patchy-particle model.

Each overhang had a 15-nucleotide poly-T spacer followed by the 8-nucleotide binding region at the 3′ flanking end. The binding-region sequences were the same on each of the three sequences in the patch, so that there was no imposed orientational control over binding of the two patches. We optimized the assigned binding regions so that for each complementary pair, the binding free energy of complementary sequences was as close as possible for all 12 binding pairs but still making the binding between overhangs that were not supposed to interact as unfavorable as possible (SM section S4).

To demonstrate the robustness of the overhang-driven assembly and inverse-design strategy, we also used an octahedral origami design in which the vertex positions did not perfectly correspond to the patch positions. This constraint in turn required that each handle was sufficiently long to adapt to the imposed geometry, which was not compatible with octahedra touching their vertices. We designed the handles with longer poly-T spacers (22 nucleotides) at each vertex to ensure that the DNA origami could arrange into the pyrochlore lattice, and used a 9-nucleotide-long binding region. The length of the spacers and sticky ends that we used in the DNA origami design was

based on an informed estimate, using the length successfully used in prior work of DNA origami assembly (*16*, *39*). We verified in patchy-particle simulations with patches placed in the octahedron vertex positions that the design with four particles species and 24 colors could still assemble into a pyrochlore lattice (SM section S1).

Both icosahedral and octahedral designs were tested in a large-scale simulation with the oxDNA model to investigate the mechanical stability and design the position and lengths of handle sequences accordingly. We assembled a pyrochlore lattice cluster measuring 2 × 2 × 2 unit cells in each dimension (total: 128 DNA origami, corresponding to over 2 two million nucleotides in the simulation). Molecular dynamics simulations were conducted for both designs (icosahedron and octahedron units) at 293 K and used to calculate the mean structure (Fig. 2, B and D). We assessed the trajectory of the center of mass (COM) for each DNA origami incorporated into the lattice and superimposed it onto the mean structure. A qualitative comparison of the relative positions of the COM trajectory and the mean structure indicated that the lattice assembled with the proposed origami design satisfied the pyrochlore geometry and was mechanically stable. We also verified that the extra single-stranded scaffold loop in the octahedral origami design (Fig. 2, A and B, and fig. S4) did not interfere with the desired pyrochlore geometry.

Experimental lattice assembly and characterizations

For each DNA origami design, we prepared each species by thermal annealing, after which, depending on the folding result of the origami, we used a purification method individually determined for each origami structure. For icosahedral DNA origami, well-folded monomeric structures, isolated by using rate-zonal purification (*40*), are preferentially used to ensure optimal lattice assembly, minimizing interference from multimeric side products. For the octahedral DNA origami, we determined that rate-zonal purification was not necessary, and simply removing the excess free staple strands with ultrafiltration was sufficient for the lattice to emerge, which was a result of the superior yield of the target monomeric structure over other structures. The four different origami species were then mixed together and annealed along a temperature ramp (SM section S2).

We monitored the size change of the system with a fast-annealing protocol using dynamic light scattering (Fig. 3A). The measured spectrum allowed us to approximately identify the temperature range at which the monomers start associating (T1) and the temperature at which the size of the assemblies reached a plateau (T2). In particular, for the octahedral origami system, T1 is 54.5°C and T2 is 53°C, whereas for the lattice assembled from icosahedral origami, it is 43° and 41°C, respectively. We then used an annealing protocol with a slow ramping rate from T1 to T2, after incubation of the system at a slightly higher temperature to dissociate any bonds between monomers (see SM section S2.3 for details). The annealing process, during which the mixed origami NPs nucleated and further crystallized, required at least 1 week for the superlattice to emerge. We suggest that both elongating and fine-tuning the annealing protocol should give rise to superlattices with enlarged sizes and improved qualities.

The assembly of octahedral and icosahedral origami systems occurred in different temperature ranges because of the different particle geometry, patch distribution, and binding strength (Fig. 3A). We observed that a higher binding strength was required for the octahedral system to assemble into the designed lattice, presumably because the icosahedron has more optimal patch positions, as supported by coarse-grained models (SM section S1).

For characterization, we coated the annealed sample with a thin layer of silica to preserve the structural details for SEM characterization (*41*). We used SEM to visualize the deposited silica-DNA hybrid structure, and the representative results are shown in Fig. 4 and SM section S3. We optimized the assembly conditions that affect the lattice formation, besides the annealing time, including origami concentration and ionic strength ([Mg^{2+}]), on the basis of the data from SEM characterization. Limited by the high binding strength, the octahedral system annealed best with the concentrations of origami of 10 nM and Mg^{2+} of 12.5 mM, to ensure the structural integrity of the nanostructure itself during lattice assembly. In comparison, with the icosahedral origami we determined (using a slow temperature ramp around the melting point) that concentrations of 10 nM

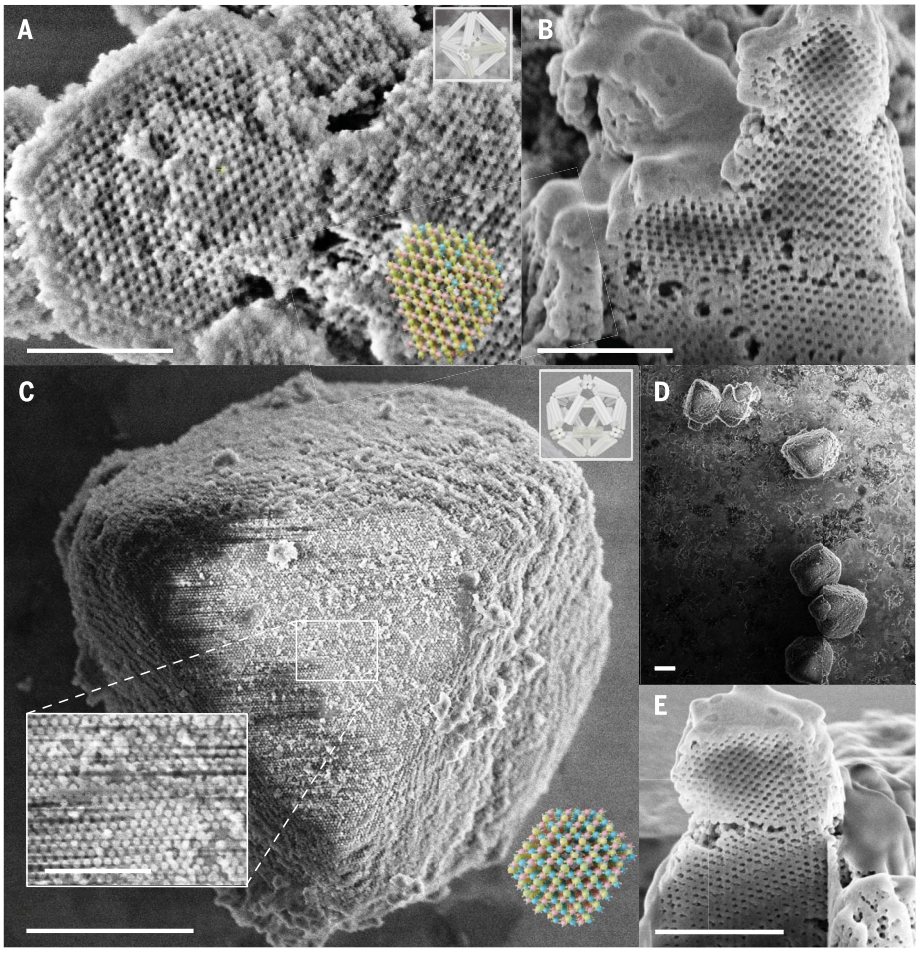

Fig. 4. SEM characterization of the fabricated pyrochlore lattice embedded with silica. Representative SEM image of the assembled pyrochlore lattice with (**A**) octahedral and (**C**) icosahedral DNA origami building blocks and (**B** and **E**) the associated cross-section of the lattice created by focused ion beam from picked smaller lattice grains. In (**D**), a typical zoomed-out view of the lattice assembled from icosahedral origami is shown. Insets for (A), (C) are models for monomer and assembled lattice fitted to the projected view. Scale bars: (A), (B), and (E), 1 μm; (C) and (D), 5 μm.

origami and 25 mM Mg^{2+} produced the best superlattice, with increased ionic strength allowing larger lattices to emerge. For both systems, clear periodicity corresponding to the pyrochlore lattices was observed. The octahedral DNA origami produced on average smaller lattice grains and more polycrystalline assemblies, with size on average 1 μm.

With icosahedral building blocks, we achieved larger and faceted lattices >5 μm. For this system, we also tried a mix-and-anneal strategy, whereby we provide mechanical agitation to the solutions while annealing. Through facilitating the diffusion of DNA origami particles and rocking the sedimented lattice in the bottom of the tube, we partially overcame the limitation of precipitation during thermal annealing. We found that this approach produced even larger lattices, with the largest dimension exceeding 20 μm (Fig. 4, C and D).

We next investigated the internal structures of the selected lattice grains with focused ion beam cross-sectional analysis. Internally associated long-range order persisted without obvious assembly defects, which confirmed the successful experimental realization of the pyrochlore lattice (Fig. 4). To confirm the lattice structure, we have further performed SAXS measurements (SM section S2.9) of the assembled lattices. For the octahedral design, we additionally attached a DNA-coated gold NP inside the origami to help the SAXS characterization. By fitting the SAXS measurements with a model of diffraction pattern for pyrochlore lattice (SM section S2.9), we obtained lattice parameters of 156.4 nm for the octahedron origami lattice and 159.1 nm for the lattice constructed from icosahedral origami. The comparison of the measured structure factor shows agreement with the one expected for the pyrochlore lattice (Fig. 3).

We also experimentally investigated two different single-species designs that satisfy the pyrochlore lattice interactions: one particle species with one self-complementary color (N1c1), and one particle species with three different colors (N1c3). Our simulations of finite-sized systems can only access kinetically preferred states, and none of the one-species systems showed successful crystallization (SM section S1). These solutions also have patches that connect particles of the same species. To prevent the aggregation of the respective DNA single strands (which represent the patch color) during the origami synthesis, we have introduced "blocker" strands to inhibit self-binding interaction, which are then strand-displaced after individual DNA origami are formed and mixed for assembly (SM section S2.5). In experiments, we observed that the structures formed by the N1c1 system lack any discernible faceting, and on a smaller scale, there is no apparent local crystalline order (fig. S22). In the case of N1c3, the larger-scale SEM visualization shows amorphous structures, whereas on smaller scales, some local crystalline order emerges in limited regions of the image, indicating poor crystallizability (fig. S23). Using the blocking strand approach, we have further tested one more design containing patches that connect to the same species: the N2c12 (two-species, 12 colors) solution (SM section S1), which is predicted to nucleate well according to our patchy-particle simulation, as its interactions avoid the misassembled states that we observed in simulations of solutions with one species only. The experimental results are shown in figs. S25 and S26 and indeed confirm the formation of large crystals with high yield.

Conclusions

We have developed a pipeline that uses multiscale modeling and optimization algorithms to design DNA nanostructures that self-assemble into the pyrochlore lattice. Our computational tools can be generalized to also design and guide the experimental realization of other types of lattices (*36*). The pipeline presented is not limited to long-range structures but can be just as easily exploited to realize finite-size assemblies (*42*) and azeotropic mixtures (*43*). The method could also be used to design initial seeding substructures for improving the yields and resulting sizes of the seeded nucleation and growth of the lattice, as well as design other sought-after lattice geometries such as clathrates (*44*).

The generality of the procedure stems from the design pipeline not relying on the specific shape of the building blocks. The geometric information of the local environment is only taken into account through a matrix of contacts. The nucleotide-level coarse-grained model is then used to verify that a particular DNA nanostructure realization is compatible with the designed patchy particle self-assembled system, so many different internal features in the designs and sizes of building blocks can be chosen. Our approach allowed us to build upon the vast literature of successful DNA nanostructure designs while being able to choose the size that provides a handle on the lattice parameters, which in turn controls the bandgap and other properties of the final lattice. The complexity of the unit cell is also not a limiting factor for the design process, because our approach is able to deal with many different building block species. The design and simulation tools are provided as free open-source software (*45*).

REFERENCES AND NOTES

1. J. D. Halverson, A. V. Tkachenko, *Phys. Rev. E Stat. Nonlin. Soft Matter Phys.* **87**, 062310 (2013).
2. M. Z. Miskin, G. Khaira, J. J. de Pablo, H. M. Jaeger, *Proc. Natl. Acad. Sci. U.S.A.* **113**, 34–39 (2016).
3. R. Kumar, G. M. Coli, M. Dijkstra, S. Sastry, *J. Chem. Phys.* **151**, 084109 (2019).
4. M. Dijkstra, E. Luijten, *Nat. Mater.* **20**, 762–773 (2021).
5. M. C. Rechtsman, F. H. Stillinger, S. Torquato, *Phys. Rev. Lett.* **95**, 228301 (2005).
6. E. Marcotte, F. H. Stillinger, S. Torquato, *Soft Matter* **7**, 2332 (2011).
7. A. Jain, J. R. Errington, T. M. Truskett, *Phys. Rev. X* **4**, 031049 (2014).
8. W. M. Jacobs, D. Frenkel, *J. Am. Chem. Soc.* **138**, 2457–2467 (2016).
9. A. Bupathy, D. Frenkel, S. Sastry, *Proc. Natl. Acad. Sci. U.S.A.* **119**, e2119315119 (2022).
10. N. Patra, A. V. Tkachenko, *Phys. Rev. E* **96**, 022601 (2017).
11. S. Mushnoori, J. A. Logan, A. V. Tkachenko, M. Dutt, *J. Chem. Phys.* **156**, 024501 (2022).
12. S. Whitelam, I. Tamblyn, *Phys. Rev. E* **101**, 052604 (2020).
13. F. Romano, J. Russo, L. Kroc, P. Šulc, *Phys. Rev. Lett.* **125**, 118003 (2020).
14. R. J. Macfarlane *et al*., *Science* **334**, 204–208 (2011).
15. T. Zhang *et al*., *Adv. Mater.* **30**, e1800273 (2018).
16. Y. Tian *et al*., *Nat. Mater.* **19**, 789–796 (2020).
17. M. He *et al*., *Nature* **585**, 524–529 (2020).
18. A. Michelson *et al*., *Science* **376**, 203–207 (2022).
19. E. Duguet, A. Désert, A. Perro, S. Ravaine, *Chem. Soc. Rev.* **40**, 941–960 (2011).
20. P. J. M. Swinkels *et al*., *Nat. Commun.* **12**, 2810 (2021).
21. I. Chakraborty *et al*., *ACS Nano* **16**, 2471–2480 (2022).
22. R. Khalaf, A. Viamonte, E. Ducrot, R. Mérindol, S. Ravaine, *Nanoscale* **15**, 573–577 (2023).
23. J. Russo, F. Leoni, F. Martelli, F. Sciortino, *Rep. Prog. Phys.* **85**, 016601 (2022).
24. P. W. K. Rothemund, *Nature* **440**, 297–302 (2006).
25. T. Ngo, C. Liddell, M. Ghebrebrhan, J. Joannopoulos, *Appl. Phys. Lett.* **88**, 241920 (2006).
26. É. Ducrot, J. Gales, G.-R. Yi, D. J. Pine, *Opt. Express* **26**, 30052–30060 (2018).
27. F. Romano, F. Sciortino, *Nat. Commun.* **3**, 975 (2012).
28. A.-P. Hynninen, J. H. Thijssen, E. C. Vermolen, M. Dijkstra, A. van Blaaderen, *Nat. Mater.* **6**, 202–205 (2007).
29. É. Ducrot, M. He, G.-R. Yi, D. J. Pine, *Nat. Mater.* **16**, 652–657 (2017).
30. J. Russo *et al*., *J. Phys. Condens. Matter* **34**, 354002 (2022).
31. N. Een, *Proc. SAT-05: 8th Int. Conf. on Theory and Applications of Satisfiability Testing* (2005), pp. 502–518.
32. E. Poppleton *et al*., *J. Open Source Softw.* **8**, 4693 (2023).
33. B. E. Snodin *et al*., *J. Chem. Phys.* **142**, 234901 (2015).
34. P. Šulc *et al*., *J. Chem. Phys.* **137**, 135101 (2012).
35. T. E. Ouldridge, A. A. Louis, J. P. Doye, *J. Chem. Phys.* **134**, 085101 (2011).
36. J. Bohlin *et al*., *Nat. Protoc.* **17**, 1762–1788 (2022).
37. J. Zhang *et al*., *J. Am. Chem. Soc.* **144**, 13146–13153 (2022).
38. Y. Tian *et al*., *Nat. Nanotechnol.* **10**, 637–644 (2015).
39. X. Yan *et al*., *J. Am. Chem. Soc.* **145**, 3978–3986 (2023).
40. C. Lin, S. D. Perrault, M. Kwak, F. Graf, W. M. Shih, *Nucleic Acids Res.* **41**, e40 (2013).
41. Y. Wang *et al*., *Nat. Commun.* **12**, 3011 (2021).
42. D. E. P. Pinto, P. Šulc, F. Sciortino, J. Russo, *Proc. Natl. Acad. Sci. U.S.A.* **120**, e2219458120 (2023).
43. C. Beneduce, F. Sciortino, P. Šulc, J. Russo, *ACS Nano* **17**, 24841–24853 (2023).
44. S. Lee, T. Vo, S. C. Glotzer, *Nat. Chem.* **15**, 905–912 (2023).
45. https://Github.com/sulcgroup/satassembly-pyrochlore

ACKNOWLEDGMENTS

We thank Y. Tian, Y. Yang, A. Neophytou, E. Seo, C. Simmons, Y. Li, L. Kroc, D. Liu, T. Liedl, and G. Posnjak for helpful discussions.
Funding: We acknowledge support from the ONR grant N000142012094 and ONR DURIP grant N000142112876. We acknowledge the use of the Extreme Science and Engineering Discovery Environment (XSEDE), which is supported by National Science Foundation grant no. TG-BIO210009. We acknowledge the use of facilities within the Eyring Materials Center at Arizona State University supported in part by NNCI-ECCS-1542160. This material is based upon work supported by the National Science Foundation under grant no. 2227650. Research reported in this publication was supported by The National Institute of General Medical Sciences of the National Institutes of Health under grant no. DP2GM132931 to N.S. The content is solely the responsibility of the authors and does not necessarily represent the official views of the National Institutes of Health. J.R. and P.Š. further acknowledge support from the Università Ca' Foscari for a Visiting Scholarship. J.R. acknowledges support from the European Research Council grant DLV-759187. J.R., L.R., and F.S. acknowledge support from ICSC–Centro Nazionale di Ricerca in High Performance

Computing, Big Data and Quantum Computing, funded by the European Union–NextGenerationEU. This research used the CMS beamline at the National Synchrotron Light Source II and Center for Functional Nanomaterials, which is a US Department of Energy Office of Science Facilities at Brookhaven National Laboratory under contract no. DE-SC0012704. D.M and O.G were supported by the US Department of Energy, Office of Basic Energy Sciences, grant DE-SC0008772. **Author contributions:** Conceptualization: H.L., J.R., F.R., L.R., M.M., P.Š. Simulations: J.R., F.R., L.R., M.M., P.Š., H.L. Experimental work: H.L., R.P.N., T.D., D.M. Data analysis: H.L., J.R., F.R., L.R., M.M., F.S., D.M., O.G., R.P.N., P.Š. Funding acquisition: O.G., J.R, N.S., H.Y., L.R., F.R., F.S., P.Š. Investigation: H.L., J.R., F.R., L.R., M.M., F.S., H.Y., D.M., R.P.N., T.D., O.G., N.S., P.Š. Project administration: H.Y., N.S., F.R., J.R., L.R., P.Š. Writing – original draft: H.L., J.R., F.R., L.R., D.M., F.S., P.Š. Writing – review and editing: H.L., M.M., J.R., F.R., L.R., D.M., F.S., N.S., O.G., P.Š. **Competing interests:** A provisional US patent has been filed based on this work. The authors declare no competing interests. **Data and materials availability:** All data needed to evaluate the conclusions in the paper are present in the paper or the supplementary materials and GitHub repository at https://github.com/sulcgroup/satassembly-pyrochlore.

SUPPLEMENTARY MATERIALS

science.org/doi/10.1126/science.adl5549
Supplementary Material Sections S1 to S4
Figs. S1 to S29
Tables S1 to S6
References (*46*–*56*)

Submitted 27 October 2023; accepted 19 March 2024
10.1126/science.adl5549